J Physiol 593.13 (2015) pp 2889–2907

The Journal of Physiology

Pronounced differences in signal processing and synaptic plasticity between piriform-hippocampal network stages: a prominent role for adenosine

Brian H. Trieu[1], Enikö A. Kramár[2], Conor D. Cox[1], Yousheng Jia[1], Weisheng Wang[1], Christine M. Gall[1,2] and Gary Lynch[1,3]

[1]*Department of Anatomy and Neurobiology, University of California, Irvine, CA, USA*
[2]*Department of Neurobiology and Behavior, University of California, Irvine, CA, USA*
[3]*Department of Psychiatry and Human Behavior, University of California, Irvine, CA, USA*

Key points

- Extended trains of theta rhythm afferent activity lead to a biphasic response facilitation in field CA1 but not in the lateral perforant path input to the dentate gyrus.
- Processes that reverse long-term potentiation in field CA1 are not operative in the lateral perforant path: multiple lines of evidence indicate that this reflects differences in adenosine signalling.
- Adenosine A1 receptors modulate baseline synaptic transmission in the lateral olfactory tract but not the associational afferents of the piriform cortex.
- Levels of ecto-5'-nucleotidase (CD73), an enzyme that converts extracellular ATP into adenosine, are markedly different between regions and correlate with adenosine signalling and the efficacy of theta pulse stimulation in reversing long-term potentiation.
- Variations in transmitter mobilization, CD73 levels, and afferent divergence result in multivariate differences in signal processing through nodes in the cortico-hippocampal network.

Abstract The present study evaluated learning-related synaptic operations across the serial stages of the olfactory cortex-hippocampus network. Theta frequency stimulation produced very different time-varying responses in the Schaffer-commissural projections than in the lateral perforant path (LPP), an effect associated with distinctions in transmitter mobilization. Long-term potentiation (LTP) had a higher threshold in LPP field potential studies but not in voltage clamped neurons; coupled with input/output relationships, these results suggest that LTP threshold differences reflect the degree of input divergence. Theta pulse stimulation erased LTP in CA1 but not in the dentate gyrus (DG), although adenosine eliminated potentiation in both areas, suggesting that theta increases extracellular adenosine to a greater degree in CA1. Moreover, adenosine A1 receptor antagonism had larger effects on theta responses in CA1 than in the DG, and concentrations of ecto-5'-nucleotidase (CD73) were much higher in CA1. Input/output curves for two connections in the piriform cortex were similar to those for the LPP, whereas adenosine modulation again correlated with levels of CD73. In sum, multiple relays in a network extending from the piriform cortex through the hippocampus can be differentiated along three dimensions (input divergence, transmitter mobilization, adenosine modulation) that potently influence throughput and plasticity. A model that incorporates the regional differences, supplemented with data for three additional links, suggests that network output goes through three transitions during the processing of theta input. It is proposed that individuated relays allow the circuit to deal with different types of behavioural problems.

DOI: 10.1113/JP270398

(Resubmitted 20 February 2015; accepted after revision 17 April 2015; first published online 22 May 2015)
Corresponding authors G. Lynch or C. Gall: Department of Anatomy and Neurobiology, University of California at Irvine, Irvine, CA 92697-1275, USA. Email: glynch@uci.edu; cmgall@uci.edu

Abbreviations A1R, adenosine A1 receptor; aCSF, artificial cerebral spinal fluid; ASSN, olfactory cortical associational system; 2-CAD, 6-amino-2-chloropurine riboside; CD73, ecto-5'-nucleotidase; DG, dentate gyrus; DPCPX, 8-cyclopentyl-1,3-dipropylxanthine; fEPSP, field EPSP; HFS, high-frequency stimulation; LEC, lateral entorhinal cortex; LOT, lateral olfactory tract; LPP, lateral perforant path; LTP, long-term potentiation; POM-1, sodium polyoxotungstate; PPF, paired-pulse facilitation; S-C, Schaffer-commissural; SO, stratum oriens; SR, stratum radiatum; TBS, theta burst stimulation.

Introduction

Processing of complex information by brain structures requires the assignment of different aspects of a given problem to different subregions. A classic example is found in the visual cortex where successive fields are used to generate progressively more holistic representations of a cue (Qin & Yu, 2013). Recent studies indicate that the hippocampus also uses its regional elements to subdivide the computations required for effective learning, with perhaps the most studied case comprising pattern separation and completion (Kesner *et al.* 2004; Leutgeb *et al.* 2007; Leutgeb & Leutgeb, 2007; Hunsaker & Kesner, 2013). Animals confronted with a novel, spatially extended environment need to construct network patterns describing cue locations that can be recalled with partial information (pattern completion), at the same time as ensuring that the encoding vectors are distinct (pattern separation). A substantial body of computational and experimental work suggests that separation is performed by modifying responses of the dentate gyrus (DG) to its entorhinal afferents, whereas completion involves synaptic changes in field CA3 (Rolls, 2013; Newman & Hasselmo, 2014).

The above interpretation of the hippocampus is largely based on anatomical data, such as the divergence of cortical inputs onto the large number of DG granule cells, the peculiar nature of mossy fibre connections and the remarkably dense commissural/associational system that occupies most of field CA3 (Boss *et al.* 1985; Ishizuka *et al.* 1990; Henze *et al.* 2000). Worthy of consideration is the possibility that regional differences in the processing of repetitive inputs arriving at characteristic hippocampal rhythms, or in the properties of learning-related synaptic changes, also contribute to local computations. Regionally distinct operations by the primary hippocampal divisions (DG, CA3, CA1, subiculum) would probably call for significant revisions to current hypotheses about the diverse roles played by the hippocampus in behaviour.

Clear evidence for differentiated functions is found in the mossy fibres where the mechanisms underlying synaptic potentiation bear little resemblance to those in other hippocampal fields (Staubli *et al.* 1990; Weisskopf *et al.* 1994; Henze *et al.* 2000; Nicoll & Schmitz, 2005). Somewhat lesser regional differences are suggested by a comparison of published studies indicating that the conditions used to induce long-term potentiation (LTP) in the perforant path projections to the DG are more severe than those for afferents of field CA1 (Larson *et al.* 1986; Abraham *et al.* 1996; Arima-Yoshida *et al.* 2011). Lacking are systematic studies directly comparing multiple measures of signal processing and plasticity at different hippocampal sites or within larger cortico-hippocampal networks. The present study addresses this issue using the piriform-hippocampal system that begins with input from the olfactory bulb and includes the piriform and lateral entorhinal cortices (LEC) along with the hippocampal connections noted above.

Theta activity (4–7 Hz) lasting for several seconds is a prominent, characteristic feature of the hippocampal and cortical EEG and is reflected in the firing patterns of individual neurons (Molter *et al.* 2012; Colgin, 2013). The rhythm appears during free exploration and correlates with various forms of learning. We therefore tested for regional differences in signal processing using 20 s trains of theta stimulation (5 Hz pulses) applied to either the lateral perforant path (LPP) inputs to the outer molecular layer of the DG or to the Schaffer-commissural (S-C) projections to the apical dendrites of field CA1. Subsequent studies tested for regional variations in the induction, expression and reversal of the memory-related LTP effect. Unexpectedly large differences between the two systems were found; further analysis identified multiple factors that probably contribute to these regional variations. The study was then extended to the lateral olfactory tract (LOT) projections to the piriform cortex and to the associational projections generated within that region. This allowed for tests of (i) the possibility that one of the two response profiles identified in the hippocampus is 'typical' for the cortical telencephalon and (ii) the mechanisms proposed to underlie the CA1 *vs.* DG differences.

Independent of cell biological substrates, the findings provide a first description of how each of four serial relays in an extended cortico-hippocampal network processes input arriving at a frequency (theta) known to be present in the network during many behaviours. These observations, in conjunction with the theta processing results for three remaining nodes in the network, were combined into a model for assessing the output of the entire system. In sum,

the present study addresses three fundamental issues: (i) the extent to which network components differ with regard to signal transformation; (ii) the processes that might account for regional variations; and (iii) the possibility that disparate operations at serial nodes combine to produce stable output.

Methods

All procedures used 6- to 8-week-old male Sprague–Dawley rats (Harlan Laboratories, Hayward, CA, USA), unless otherwise noted, in accordance with UK regulations, the NIH Guide for the Care and Use of Laboratory Animals, and institutionally approved protocols.

Extracellular field recordings

Rats were decapitated and the brain was quickly submerged in oxygenated, ice-cold, high magnesium artificial cerebral spinal fluid (aCSF) containing (in mM): 124 NaCl, 3 KCl, 1.25 KH_2PO_4, 5 $MgSO_4$, 26 $NaHCO_3$ and 10 dextrose. For the hippocampus, acute slices were prepared from the middle third of the structure's septotemporal axis, using a McIlwain tissue chopper (Ted Pella, Redding, CA, USA), and transferred to an interface recording chamber (31 ± 1^{o}C; 95% O_2/5% CO_2) (Kramar *et al.* 2002; Kramar & Lynch, 2003). Slices were continuously perfused with preheated oxygenated aCSF containing (in mM): 124 NaCl, 3 KCl, 1.25 KH_2PO_4, 1.5 $MgSO_4$, 26 $NaHCO_3$, 2.5 $CaCl_2$ and 10 dextrose at a rate of 60–70 ml h^{-1}. Recordings began ≥1.5 h after transfer to the chamber.

Four hippocampal pathways were evaluated in these experiments (Fig. 1). For studies of the S-C innervation of CA1, field EPSPs (fEPSPs) were recorded in the apical dendritic field by positioning a glass electrode (2 M NaCl, 2–3 MΩ) in CA1b stratum radiatum (SR). Test pulses (0.05 Hz) were delivered to the S-C projections using a bipolar stimulating electrode (twisted nichrome wire, 65 μm) in CA1c. In the CA3 associational system, stimulating and recording electrodes were placed in SR of CA3b and CA3a, respectively. For analysis of the LPP innervation of the DG molecular layer, stimulating and recording electrodes were positioned in the distal third of the molecular layer (inner leaf), adjacent to the hippocampal fissure. Evoked responses in the outer molecular layer were initially tested with paired-pulse stimuli (40 ms interpulse interval) to confirm the specificity of potentials to the LPP (Christie & Abraham, 1994). Mossy fibre field potentials were recorded from CA3c stratum lucidum with stimulating electrodes placed in the subgranular zone of the DG. Stimulation intensities in all cases were adjusted to yield response amplitudes approximately 50–60% of the maximum spike-free fEPSP. The intensity was adjusted to 25–35% of the maximum spike-free response in experiments using an adenosine A1 receptor (A1R) antagonist.

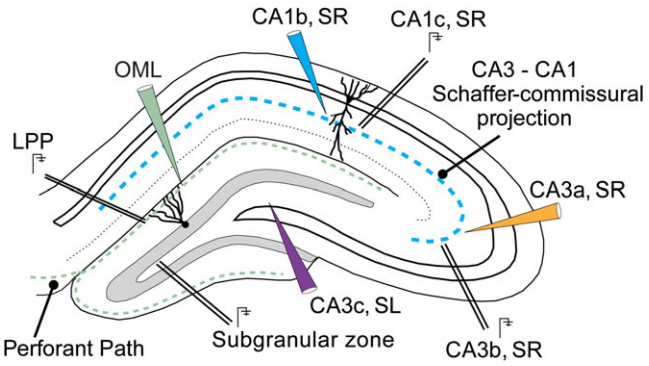

Figure 1. Schematic of a hippocampal slice showing electrode placements
Stimulating (parallel lines) and recording electrodes (cones) were positioned in CA1 SR, CA3 SR, DG outer molecular layer (OML) and subgranular zone to evaluate responses to S-C, CA3 associational, LPP and mossy fibre innervation, respectively.

Input/output curves for the different synaptic populations were generated using stimulation currents from 10–100 μA. To evaluate paired-pulse facilitation (PPF), two stimulation pulses were delivered at intervals of 40, 60, 100 and 200 ms and the initial slope of the responses was measured. LTP was induced in the LPP by delivering a single train of high-frequency stimulation (HFS) at 100 Hz for 500 ms after a minimum of 20 min of stable baseline recording. Stimulus duration and intensity were increased by 100% and 50% of baseline levels, respectively, to achieve significant and stable LTP (Bramham & Sarvey, 1996; Suzuki & Okada, 2007). Tests for the accuracy of returning current to baseline levels were conducted on control slices using the slopes of 10 averaged potentials collected before increasing the current and then after restoring it to baseline; slopes of the fEPSPs differed by less than ± 2%. In separate experiments, three theta pulse stimulation trains (5 Hz, 300 pulses), spaced by 1 min, were delivered to non-potentiated and potentiated responses in an attempt to disturb baseline synaptic transmission or reverse LTP (Kramar & Lynch, 2003).

For studies of the anterior piriform cortex, sagittal slices were prepared using a vibrating tissue slicer (Model: VT1000S; Leica, Wetzlar, Germany). We confirmed that the cutting technique did not measurably affect outcomes by testing field CA1 and LPP using the same vibratome procedure employed for the piriform cortex. The brain was separated on the mid-sagittal plane and both hemispheres were sectioned at a thickness of 320 μm. Slices with a visibly attached LOT were transferred to an interface recording chamber containing normal aCSF (as used with hippocampal slices). At least 2 h later, bipolar stainless steel stimulating electrodes (diameter 25 μm; FHC Inc., Bowdoin, ME, USA) and single glass recording

electrodes (2 M NaCl; 2–3 MΩ) were positioned in piriform cortex layers 1a and 1b to activate and record LOT and associational (olfactory cortical associational system; ASSN) afferent responses, respectively. Isolated fEPSPs in each layer were confirmed by applying paired-pulses. In agreement with previous studies, LOT responses displayed pair-pulse facilitation, whereas ASSN responses exhibited paired-pulse depression (Gocel & Larson, 2013).

For studies of LEC, horizontal slices located between –6.10 mm and −7.60 mm ventral to bregma (Paxinos & Watson, 1986) were sectioned at a thickness of 370 μm using the Leica vibrating tissue slicer (as described above). Experiments began ≥1.5 h after transfer to an interface chamber containing normal aCSF. A single glass recording electrode (2 M NaCl; 2–3 MΩ) and stimulating electrode (twisted nichrome wire, 65 μm) were placed in LEC layer 1b. To confirm correct electrode placement, slices were stained with cresyl violet and examined after the experiment.

In all instances, initial slopes and amplitudes were measured from digitized fEPSPs (NACGather 2.0; Theta Burst Corp., Irvine, CA, USA). Facilitation of responses to theta pulse trains was analysed using an in-house MATLAB script (MathWorks Inc., Natick, MA, USA) and normalized to the amplitude of the first pulse within the train. All measures are reported as the group mean ± SEM.

Whole-cell recordings

Hippocampal slices used for whole-cell recordings were prepared from 3- to 4-week-old rats as described previously (Colgin *et al.* 2005). Slices were placed in a submerged recording chamber continuously perfused at 2–3 ml min^{-1} with oxygenated (95% O_2/5% CO_2) normal aCSF (as above) at 32°C. Whole-cell recordings (Axopatch 200A amplifier; Molecular Devices, Sunnyvale, CA, USA) were made with 4–7 MΩ recording pipettes filled with a solution containing (in mM): 130 $CsMeSO_4$, 10 CsCl, 8 NaCl, 10 Hepes, 0.2 EGTA, 5 QX-314, 2 Mg-ATP and 0.3 Na-GTP. Osmolarity was adjusted to 290–295 mOsm l^{-1} and pH was buffered at 7.25. Synaptic currents were elicited by stimulation of the LPP. EPSCs recorded from DG granule cells were clamped at −70 mV in the presence of 50 μM picrotoxin. After a stable 10 min baseline, LTP was induced using a pairing protocol of 2 Hz stimulation for 75 s at a holding potential of −10 mV. Previous studies have shown that this protocol is not significantly different from HFS and is sufficient to produce NMDA-dependent LTP in clamped neurons (Manabe *et al.* 1993).

Drug application

Drugs were made fresh on the day of use and introduced to the bath (6 ml h^{-1}) via an independent perfusion line using a syringe pump (KD Scientific Inc., Holliston, MA, USA). The A1R antagonist 8-cyclopentyl-1,3-dipropylxanthine (DPCPX; Abcam, Cambridge, MA, USA) was prepared in 100% DMSO and diluted to a final concentration of 500 nM in aCSF (DMSO at 0.02%). The adenosine analogue, 6-amino-2-chloropurine riboside (2-CAD; R&D Systems, Minneapolis, MN, USA), was dissolved in aCSF to a final concentration of 400 μM to achieve rapid but brief saturation of adenosine receptors; accordingly, infusion was limited to 2 min. For experiments involving 2-CAD-mediated inhibition of LTP stabilization, infusion started 3 min prior to HFS. The perfusion system is such that 4–5 min are required before 2-CAD begins to depress synaptic responses; thus, the agent in the present study reached physiologically significant concentrations at 1–2 min after the induction of LTP. The NTPDase inhibitor sodium polyoxotungstate (POM-1; Tocris Bioscience, St Louis, MO, USA) and opioid receptor antagonist naloxone hydrochloride dihydrate (Sigma, St Louis, MO, USA) were infused to a bath concentration of 30 μM and 20 μM, respectively.

Immunohistochemistry

Eighteen rats were killed with an overdose of Euthasol (Virbac, Fort Worth, TX, USA) and intracardially perfused with 4% paraformaldehyde; tissue sections (30 μm, coronal) were prepared on a freezing microtome and processed free floating for immunofluorescence using overnight (4°C) incubation with mouse antisera to ecto-5'-nucleotidase (CD73) (dilution 1:800; clone 5F/B9; BD Biosciences Clontech, Palo Alto, CA, USA) alone or in combination with goat anti-calretinin (dilution 1:2000; AB5054; Millipore, Billerica, MA, USA); secondary antisera included AlexaFluor594 donkey anti-mouse IgG and AlexaFluor488 donkey anti-goat IgG (dilution 1:1000; Invitrogen, Carlsbad, CA, USA) (Rex *et al.* 2009). For regional measures, tissue from three 50-day-old rats was processed together and immunolabelling densities were assessed for five sections per rat from epifluorescence images captured at 10× [6000B microscope (Leica) with a CMOS camera (PCO Scientific, Kelheim, Germany) and Metamorph acquisition software (Molecular Devices)], using ImageJ (Bethesda, MD, USA) (Preibisch *et al.* 2009; Schneider *et al.* 2012). Multiphoton images were obtained using a Thor A-Scope (ATN Corp., San Francisco, CA, USA) and 63× (1.4NA) objective, Thorimage, version 1.4, for acquisition (ATN Corp.) and red imaging at 825 nM.

Modelling

The basic model of signal transduction through a circuit was created using Python, version 2.7.4 (https://www.

python.org), NumPy (http://www.numpy.org) and Brian simulator, version 2 (http://briansimulator.org) (Stimberg *et al.* 2014). The framework of Brian simulator allows the user to define, integrate and then simulate spiking neural networks by modifying the number of cells per stage, speed of repolarization, strength of each synapse, decay tau for EPSPs/IPSCs, synaptic strength change over time and connectivity of the regions. All synapses adjusted their strength over time in accordance with piecewise equations, as described below. As with most biologically motivated network models, compromises were necessitated by the number of neurons that can be realistically simulated; in the present case, 200 cells for all nodes except field CA3 ($n = 400$). Accordingly, all values incorporated into the system are relative to each other. Firing rates were governed by three factors in addition to the number and strength of active inputs: (i) an inhibitory period after a spike reflecting the time frame of IPSCs and after hyperpolarization; (ii) the tau for membrane repolarization after a spike; and (iii) the decay tau of EPSPs and IPSPs.

Connectivity (i.e. the probability that a given input axon will contact a given target cell) was based on anatomical data (number of afferents *vs.* number of targets) (Boss *et al.* 1985; Ishizuka *et al.* 1990; Kerr *et al.* 2007). Accordingly, it was higher in CA3-CA3 and CA3-CA1 than for piriform and DG connections and higher still in the mossy fibre connections. Synaptic strengths (i.e. the level needed to fire a target neuron) were equivalent for all contacts except the mossy fibres, which, based on published reports, were given 3× potency relative to all other sites (Henze *et al.* 2000). IPSCs in CA3 were represented as a spread of suppression from an active neuron to its neighbours. These connections were given twice the delay of the CA3-CA3 excitatory connections. The time varying the strength of connections at each step in the network during theta was based on the experimental results described below. The empirical values were smoothed and then converted into piecewise equations for time *vs.* strength and these were implemented into single synapses. For graphical purposes, the results from the simulation are described as the percentage of peak firing rates over a 20 s theta period.

The model in its entirety is available at: http://modeldb.yale.edu/181032.

Statistical analysis

All results are presented as the mean ± SEM. Statistical significance ($P < 0.05$) was evaluated using Student's t test or two-way ANOVA as indicated. GraphPad Prism (GraphPad Software Inc., San Diego, CA, USA) was utilized for the analysis.

Results

Processing of theta pattern input differs markedly between the DG and field CA1

Temporally extended periods of theta activity (4–7 Hz) are a characteristic feature of the hippocampus. We used 5 Hz trains to test whether the pattern is processed differently by the DG *vs.* field CA1. S-C responses in CA1 exhibited a rapid rise between the first and second pulses, followed by less marked, progressive increases for the next six or seven pulses. Next, there was a decline over the subsequent 15 pulses and then a second, more slowly developing, increase that reached its maximum at approximately pulse number 70 (Fig. 2*A*). Notably, the facilitation did not persist after the 20 s of repetitive activation and, indeed, was typically followed by a weak and transient (<60 s) depression of baseline responses; post-theta depression is discussed below. The same theta stimulation produced very different effects when applied to the LPP, a primary afferent to the DG outer molecular layer. The second response exhibited the same increase as found in field CA1, although subsequent potentials were progressively less facilitated; a secondary enhancement was not present (Fig. 2*B*). Recordings from the CA1 cell body layer showed that the enhanced S-C responses produced by 5 Hz stimulation were sufficient to trigger cell discharges and, in some cases, population spikes across the entire duration of the episode (Fig. 2*A*, inset). Neuronal discharges were not evident during the LPP theta train. The medial perforant path, which conveys non-olfactory information to hippocampus, did not facilitate during theta stimulation; the second response was not elevated above baseline and subsequent reponses were progressively smaller (data not shown). This peculiar pattern is probably related to the unusual paired pulse depression found in this projection (Christie & Abraham, 1994).

In an effort to identify factors involved in the regionally differentiated processing of theta activity, we repeated the above experiments on LPP and CA1 on different slices using pairs of stimulation pulses (interpulse interval of 40 ms) separated by the 200 ms period of theta frequency. This paradigm allowed us to assess PPF, which is evident at 40 ms delays, throughout the train. Numerous studies have shown that enhancing release to a first pulse results in decreased facilitation of the second response, with the interpretation being that greater depletion of available vesicles by the first (enhanced) release event reduces the pool available for the second response (Manabe *et al.* 1993; Debanne *et al.* 1996). The PPF protocol thus provides a test of whether increased transmitter release contributes to the response facilitation found during single pulse theta stimulation. In field CA1, PPF inversely mirrored the single pulse response curves described in Fig. 2*A*: facilitation fell precipitously during the initial

phase of the train, as expected if increased release was responsible for the observed rise in single fEPSPs, recovered over the next twenty pairs, and then slowly fell again (Fig. 2*C*). The values for the amplitude of theta pulse responses and PPF were strongly, and negatively, correlated and highly significant ($r = -0.801$, $r^2 = 0.642$; $P < 0.0001$). These results agree with the hypothesis that the time varying responses generated by S-C synapses to a theta train reflect changes in transmitter release.

Over time, changes in PPF in the LPP differed markedly from those described for the S-C innervation of CA1. The sharp decrease from the first to the second pulse was comparable in the two systems, although this was followed by a slow and steady decline for the remainder of the train, with PPF no longer present by the fifth to sixth pulse (Fig. 2*D*). The differences between PPF curves in CA1 and DG were highly significant ($P < 0.0001$, two-way repeated measures ANOVA, $F_{992871} = 4.34$). In sum, the PPF results strongly suggest that S-C terminals possess delayed transmitter mobilization capacities lacking in the LPP.

The LPP is unusual for hippocampal projections in that it contains high concentrations of enkephalin and there is good evidence that the opioid plays an important role in the induction of LTP by depressing GABAergic terminals and thus feedforward inhibition (Breindl *et al.* 1994; Bramham & Sarvey, 1996). We tested the possibility that it also dampens facilitation during theta stimulation. The sigma opioid receptor antagonist naloxone was infused for 40 min prior to the delivery of theta stimulation at a concentration confirmed to block LTP; the pretreatment had no evident effect on the facilitation curve ($P > 0.50$, two-way ANOVA, $F_{99792} = 0.49$ for comparisons made before *vs.* during drug infusion).

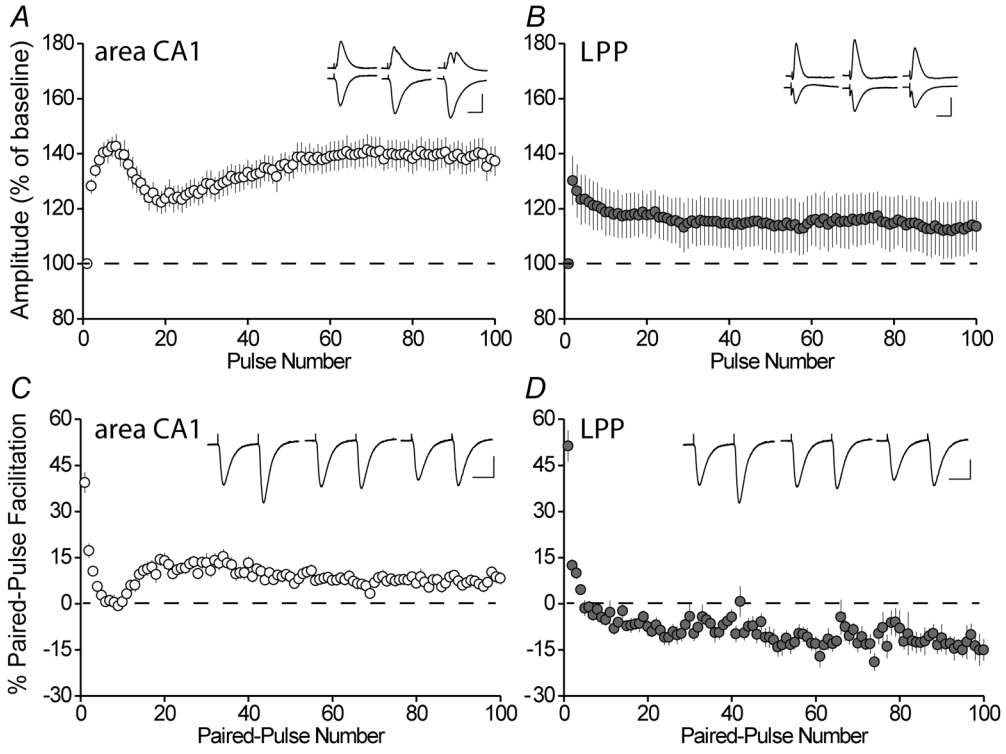

Figure 2. Theta processing differs between S-C and LPP synapses
A, changes in the amplitude of fEPSPs elicited by the S-C projections to field CA1 SR during a 20 s train of 5 Hz stimulation (100 pulses) expressed as a percentage of the pre-train baseline (mean ± SEM; $n = 7$). Note the biphasic facilitation pattern. Inset: representative traces of pyramidal cell body (top) and dendritic/SR (bottom) responses to the first, eighth and last pulse of the theta train; spikes are present on the second and third traces. Scale bar = 1 mV/10 ms. *B*, frequency facilitation of dendritic fEPSP LPP responses during a 20 s theta train ($n = 7$); facilitation occurred to the same degree as in CA1 for the second pulse but decreased steadily throughout the remainder of the train. Inset: representative traces of cell body and dendritic responses at the same points in the train as in (*A*); spikes were not evident. Scale bar = 1 mV/10 ms. *C*, paired-pulses spaced by 40 ms were given at the theta rhythm (200 ms intervals) for 20 s in CA1 ($n = 16$). The percentage increase of the second response in the pair relative to the first is shown. Changes in percentage facilitation during the train are the opposite of those for the single pulse responses shown in (*A*) ($r = -0.831$). Inset: representative paired-pulse responses recorded from the dendritic field at the time points shown in (*A*). Scale bar = 0.5 mV/10 ms. *D*, the same stimulation (as in C) applied to the LPP ($n = 15$) elicited decreasing PPF throughout the train. Inset: as in (*C*). Scale bar = 0.25 mV/10 ms.

DG *vs.* CA1 differences in the threshold for LTP

The stimulation conditions used to induce potentiation in the perforant path are typically more extreme than those required for field CA1 (Abraham *et al.* 1996; Kramar *et al.* 2012), suggesting that the threshold for LTP is higher in the former area. We carried out a formal comparison to test this conclusion. In field CA1, a single train of ten theta bursts (100 Hz bursts of four pulses, separated by 200 ms) causes a rapid and pronounced increase in field EPSPs that decays to a stable plateau ∼50% above baseline (Kramar *et al.* 2012). The same stimulation applied to the LPP had very little effect on subsequent responses elicited by single pulses; percentage LTP at 60 min after the theta burst train was 4 ± 3% (Fig. 3*A*, triangles). HFS (100 Hz for 500 ms) delivered at baseline currents also failed to induce LTP in the DG (Fig. 3*A*, open circles). Successful induction using the same protocol was achieved, however, by increasing the stimulation duration and intensity by 100% and 50%, respectively, resulting in stable potentiation at 140 ± 5% of baseline (Fig. 3*A*, filled circles). These observations confirm that the DG has an elevated threshold for LTP, relative to field CA1 in hippocampal slices.

The above results prompted us to re-examine the responses of the two areas to their respective inputs. Single pulse stimulation of the LPP produced fEPSPs of a magnitude and shape comparable to those described previously (Colino & Malenka, 1993; Macek *et al.* 1996; Colgin *et al.* 2003). The responses typically had a larger fibre volley than was recorded in the S-C system, suggesting that stimulation of a greater number of axons is needed

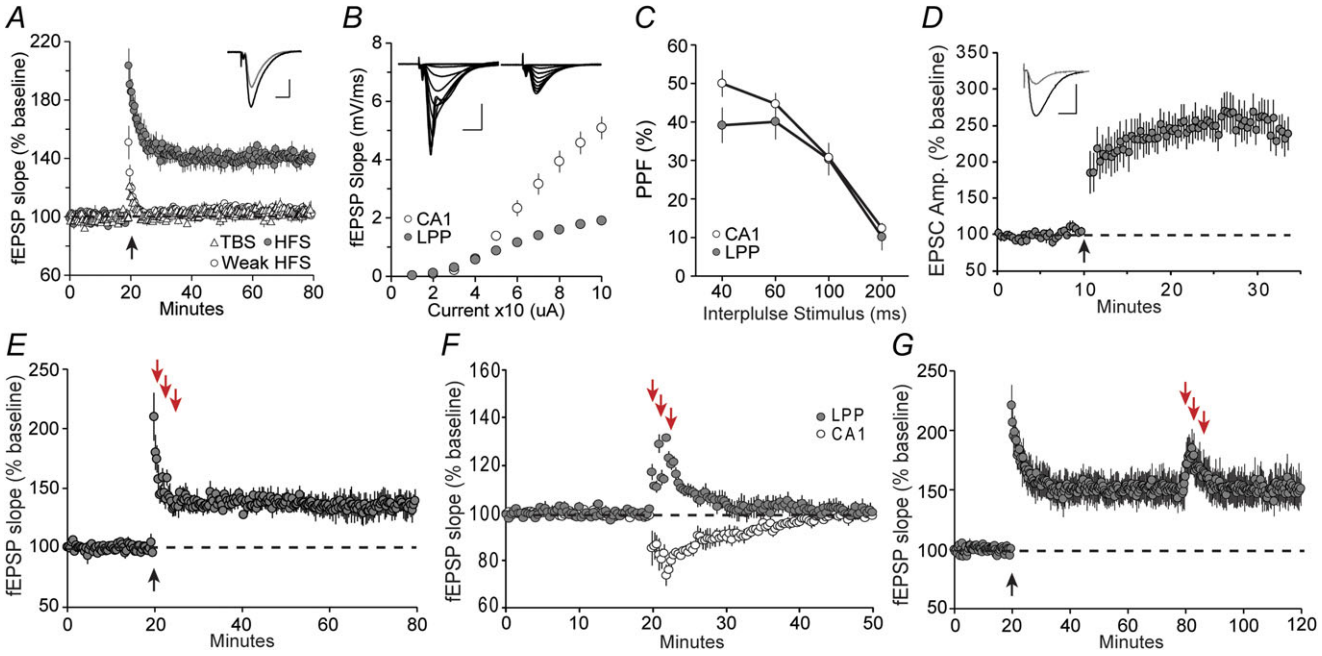

Figure 3. Regional differences in LTP induction and stabilization
A, after 20 min baseline fEPSP recordings, the LPP was stimulated (upward arrow) with either theta burst stimulation (TBS; 100 Hz bursts of four pulses, separated by 200 ms, triangles), weak HFS (one 100 Hz train lasting 0.5 s at baseline stimulation strength, open circles) or HFS (one 100 Hz train lasting 0.5 s with pulses at 200% of the duration and 150% of the intensity of baseline stimulation, filled circles). HFS produced stable LTP (140 ± 4% of baseline, $n = 6$), whereas the weak HFS ($n = 6$) and TBS ($n = 6$), which is effective for field CA1, did not. Inset: representative traces collected during baseline (grey) and 20 min after HFS (black). Scale bar = 0.5 mV/5 ms. *B*, input/output curves compare the initial slope of the fEPSP with the amount of current delivered to S-C innervation of CA1 ($n = 8$) and the LPP ($n = 16$). Inset: representative traces for CA1 (left) and LPP (right). Scale bar = 2 mV/5 ms. *C*, PPF of the initial slope of the synaptic response was comparable for CA1 ($n = 6$; open circles) and LPP ($n = 8$; filled circles) at all interpulse intervals. *D*, whole-cell recordings from granule cells before and after delivery (upward arrow) of a single 2 Hz train of 150 pulses to the LPP. Cells were held at −10 mV during the train. Percentage LTP (250 ± 23% of baseline, $n = 10$) was comparable to that reported for CA1 after the same stimulation applied to S-C afferents. Inset: representative traces of baseline (grey) and potentiated (black) EPSCs. Scale bar = 200pA/20 ms. *E*, three 1 min long theta trains (downward arrows) failed to reverse LTP in the LPP when applied 1 min after LTP-induction ($n = 4$). *F*, three 1 min long theta trains (separated by 1 min) immediately reduced the magnitude of baseline synaptic responses in CA1 ($n = 5$) at the same time as enhancing LPP responses in the DG ($n = 6$). Responses in both regions returned to baseline over the remaining 30 min. *G*, three theta trains applied to the LPP delivered 60 min after induction failed to reverse LTP in the DG but, instead, caused a transient enhancement, as shown in (*F*).

to produce a robust synaptic potential in the DG. As anticipated from this, input/output (current *vs.* fEPSP slope) curves for the two systems were markedly different: stimulation of increasing numbers of fibres produced a greater and more rapid rise in slope in CA1 than in the DG outer molecular layer ($P < 0.0001$, two-way ANOVA, $F_{9210} = 48.78$) (Fig. 3*B*). One interpretation of these findings is that the spread of axons to the target recording area is greater for the LPP than for S-C projections, as is supported by anatomical studies (Han *et al.* 1993; Megias *et al.* 2001). This also agrees with the general idea (Boss *et al.* 1985; Leutgeb *et al.* 2007) that the LPP is a divergent system with greater numbers of target neurons in the DG than input neurons in the entorhinal cortex; this is not the case for the S-C system where neuron numbers in CA3 and CA1 are approximately equivalent (Ishizuka *et al.* 1990).

We also compared PPF curves between the two fields using interpulse intervals of 40, 60, 100 and 200 ms. Responses for field CA1 and the LPP were not reliably different, indicating that baseline release kinetics are similar in the two regions (Fig. 3*C*).

Activation of NMDA receptors at single synapses is facilitated by depolarization of local dendritic branches via synchronous stimulation of neighbouring inputs, which would require the firing of a greater number of axons, and thus an apparently elevated threshold for LTP induction in a diffusely connected system. Notably, previous studies have found that the mEPSCs are not smaller in the DG than in field CA1 (Min *et al.* 1998; Jain *et al.* 2012; Zhang *et al.* 2015) and so variations in responses to single terminals are probably not a factor in the LTP threshold differences. The above divergence hypothesis predicts that LTP induction would be comparable in CA1 and the DG under conditions in which the voltage block on NMDA receptors is reduced; this can be accomplished by raising the membrane potential during whole-cell recording. We conducted such a clamp experiment and found that the stimulation parameters conventionally used to induce LTP in field CA1 (Manabe *et al.* 1993) were fully effective for the granule cells of the DG (Fig. 3*D*). This is in agreement with past studies indicating that synaptic plasticity at the LPP-DG synapse is NMDA receptor-dependent (Colino & Malenka, 1993; Niewoehner *et al.* 2007). It is interesting to note that LTP is readily induced *in vivo* by short trains of high-frequency bursts delivered to the angular bundle (Bramham *et al.* 1991; Christie & Abraham, 1994). Such stimulation probably engages a much broader population of perforant path axons than the punctate stimulation proximal to a recording site used in slice experiments and thus overcomes the divergence problem.

Processes that reverse LTP in field CA1 are not present in the DG

We next tested for regional differences in a second aspect of LTP; namely, its vulnerability to reversal by theta pulse stimulation applied shortly after induction. Previous studies have described this effect for the S-C projections in anaesthetized rats (Barrionuevo *et al.* 1980), chronic recordings in alert rats (Staubli & Lynch, 1990) and hippocampal slices (Larson *et al.* 1993). Reversal (depotentiation) has also been reported for the perforant path, although only after intense stimulation (Abraham *et al.* 1996; Martin, 1998) conditions that make it difficult to distinguish erasure from long-term depression (Dunwiddie & Lynch, 1978; Dudek & Bear, 1992). Therefore, we re-examined the point by applying three 5 Hz trains (separated by 1 min), comprising a protocol that does not cause LTD but nonetheless erases LTP in CA1, to the LPP starting 60 s after HFS. The 5 Hz trains had no effect on LTP in the DG (Fig. 3*E*).

The above results indicate that theta pulse stimulation either (i) triggers release of different factors in CA1 than in DG or (ii) LTP reversal machinery found in CA1 is missing from the DG. We investigated the first idea by comparing the effects of 1 min theta trains on subsequent baseline synaptic responses in the two regions. The first S-C train was followed by a reduction in fEPSP slope elicited by single S-C pulses that persisted throughout the next minute; subsequent trains added to the depression, resulting in a peak suppression of 26 ± 5% (Fig. 3*F*). The depression dissipated during the 30 min after the last train. The results for the DG were unexpected: responses recorded immediately after the trains were increased above baseline (maximum: 32 ± 1%; $P < 0.00001$ *vs.* S-C, two-tailed *t* test) with ∼20 min required for a return to baseline (Fig. 3*F*). It should be noted that the responses *during* the train were altered as shown in Fig. 2*A*. Thus, the signalling events of some minutes in duration set in motion by extended theta trains are very different in CA1 and the DG; this observation plausibly relates to the presence *vs.* absence of a capacity for erasing newly induced LTP.

The LTP-reversal effect in CA1 becomes progressively less pronounced with time after theta burst stimulation, with no reversal occurring after delays of 15–30 min (Kramar & Lynch, 2003). We tested whether LPP potentiation follows an opposite rule in which 5 Hz trains become effective after long delays. This was not the case: the stimulation applied 1 h post-induction produced the same transient increase found for baseline responses (Fig. 3*G*). Collectively, these results indicate marked regional differences in both the induction and later malleability of LTP.

Pronounced regional differences in adenosine-mediated modulation of signal processing and LTP

Theta stimulation, albeit under conditions different from those used in the present study, increases extracellular

levels of adenosine in field CA1 (Abraham & Huggett, 1997; Huang *et al.* 1999). Adenosine acting through A1R is known to reduce glutamate release (Dunwiddie & Haas, 1985; Wu & Saggau, 1994). We used the A1R antagonist DPCPX at a concentration found in pilot studies to be approaching the threshold for affecting baseline responses in CA1: 500 nM increased CA1 fEPSPs in two of nine slices but did not affect baseline responses in the LPP. This concentration was then used to test if theta trains differentially engage synaptic adenosine signalling in the

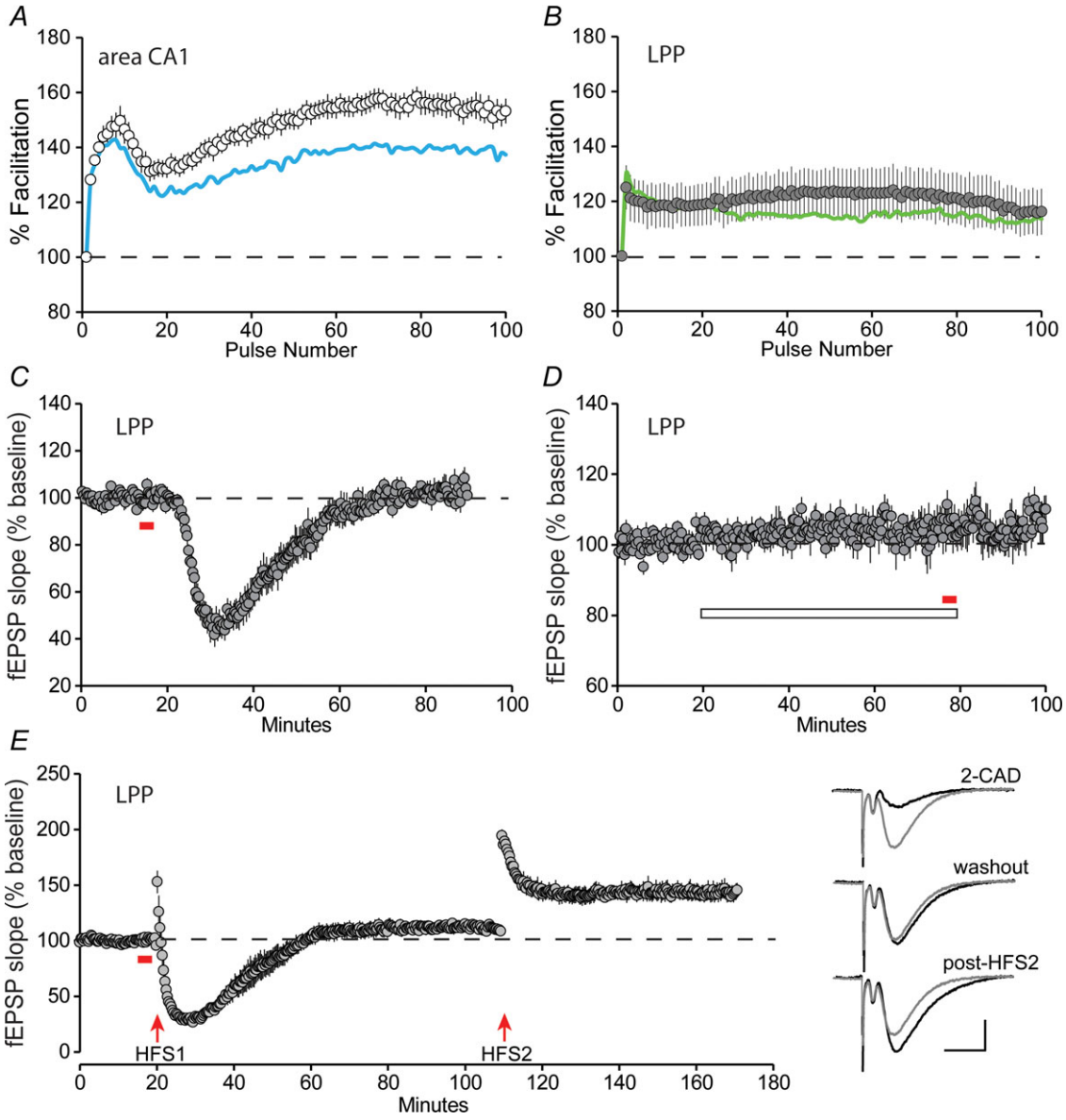

Figure 4. LPP fEPSPs respond to agonists but not antagonists of the A1R
A, a 20 s theta train was delivered to S-C projections after 1 h pretreatment with the A1R antagonist DPCPX (500 nM): percentage facilitation of field CA1 fEPSP amplitude relative to pre-train baseline responses are plotted (open circles; $n = 7$). The biphasic response facilitation profile was similar to that observed without DPCPX present (indicated with continuous line) but responses were clearly amplified. *B*, same paradigm as in (*A*) but applied to the LPP; DPCPX (filled circles, $n = 7$) had little effect on responses relative to those obtained in the drug-free condition (continuous line). *C*, infusion of the A1R agonist 2-CAD (200 μM; solid bar) caused an immediate depression in the LPP fEPSP slope that gradually recovered to baseline values ($n = 5$). *D*, pretreatment with DPCPX (open bar) completely blocked 2-CAD-induced depression of LPP synaptic responses ($n = 5$). *E*, 2-CAD applied for 2 min (filled bar) immediately prior to 100 Hz stimulation (HFS1) (i.e. to arrive immediately after the train) disrupted induction of LTP in the LPP. After 60 min drug washout, a second 100 Hz stimulation train (HFS2) produced normal LTP ($n = 5$). Traces on the right show LPP responses during baseline recordings (grey) and during 2-CAD-induced depression, washout and post-LTP induction (latter three in black). Scale bar = 0.5 mV/10 ms.

two regions. DPCPX enhanced CA1 responses throughout the train, with increases becoming particularly evident (~60%) after the first 15 pulses ($P < 0.0001$, two-way repeated measures ANOVA, $F_{981176} = 1.87$) (Fig. 4*A*). However, the antagonist had little influence on LPP responses, except for a slight facilitation halfway through the theta train (Fig. 4*B*). Indeed, by subtracting baseline facilitation curves from drug-treated curves, the difference in DPCPX actions on the two projection systems was highly significant ($P < 0.0001$, two-way repeated measures ANOVA, $F_{2993588} = 1.664$, fEPSP amplitudes were normalized to the first fEPSP of the theta train before subtraction). It thus appears that two variables (i.e. neurotransmitter mobilization and adenosine modulation) distinguish theta processing by field CA1 *vs.* the DG.

Adenosine also suppresses the post-synaptic signalling cascades necessary for LTP stabilization (Rex *et al.* 2009). The regionally distinct adenosine responses described above could thus explain why LTP reversal is prominent in CA1 but not in the DG. However, as noted above, it remains possible that essential machinery for erasure is missing from the dentate. A1Rs are present at high concentrations in the DG molecular layer (Lee *et al.* 1986; Rex *et al.* 2005), although it is not known whether or how they influence baseline physiology or LTP. We tested this using brief infusion of the adenosine analogue 2-CAD. The A1R agonist, after a delay of 2–3 min, caused a rapid and pronounced decrease in LPP fEPSPs that fully reversed upon washout (Fig. 4*C*) and was similar to that described for field CA1 (Dolphin, 1983; Arai *et al.* 1990; Demendonca & Ribeiro, 1990). The depression in the DG was evident in the initial portion of the fEPSP, did not involve a detectable change in the fibre volley, and was fully blocked by pretreatment with DPCPX (Fig. 4*D*). Moreover, brief 2-CAD infusions timed to arrive after HFS blocked the stabilization of LTP in the LPP: the post-induction treatment produced the expected depression of responses, followed by recovery to a stable level that was only slightly above baseline ($11.7 \pm 3.4\%$; $P = 0.028$, paired t test). A second HFS train applied after 2-CAD washout resulted in a typical LTP profile: a sizable amount of short-term potentiation followed by decay to a plateau that was substantially higher than baseline ($44.0 \pm 6.4\%$; $P < 0.007$, paired t test) (Fig. 4*E*). Thus, post-induction adenosine infusion largely eliminates LTP in the DG as it does in field CA1. Accordingly the failure of theta stimulation to reverse LTP in the LPP is not due to the absence of adenosine-driven machinery for disrupting stabilization of the potentiation effect.

An element for activity-driven adenosine accumulation is lower in the DG than in CA1

The above results indicate a failure of adenosine release or breakdown of secreted nucleotides to adenosine, or both, during 5 Hz LPP stimulation. In accordance with the latter possibility, previous studies using histochemistry obtained evidence that the activity of CD73, the extracellular rate-limiting enzyme in the conversion of released ATP to adenosine (Cunha, 2001; Lovatt *et al.* 2012), is greater in CA1 than in the DG molecular layer (Lee *et al.* 1986; Schoen & Kreutzberg, 1994). Whether this reflects reduced CD73 expression in the DG or an absence of factors required for enzyme activation is not known. We therefore used immunostaining to evaluate the distribution of CD73 within and between hippocampal subfields and thus to test the specific prediction that concentrations of the nucleotidase are low in the LPP terminal zone.

CD73 immunolabelling was extremely dense in stratum oriens (SO) of CA1, very low in the pyramidal cell body layer and, again, very high in SR. Stratum lacunosum-moleculare, which receives input from entorhinal cortex, had noticeably lower concentrations than other CA1 lamina (Fig. 5*A*). Labelling was much lower in the molecular layer of the DG than in the primary dendritic lamina of CA1 (Fig. 5*B*). The granule cell layer was almost devoid of immunostaining, although the infragranular zone of the hilus, which contains large numbers of granule cell axon collaterals and scattered neurons of diverse types, had significant concentrations. Possibly related to this, the mossy fibre zone within field CA3 had reliable, although not particularly dense, immunolabelling. Interestingly, there were no evident differences between the inner, middle, and outer molecular layers of the DG (Fig. 5*B*).

Densitometric measurements confirmed the above described subfield differences in CD73 levels. The immunofluorescence intensity was measured for sample fields indicated by boxes in Fig. 5*B*, expressed as the density above corpus callosum values for the same tissue section, and averaged across five sections per rat. This quantification demonstrated that immunolabelling was comparably dense in CA1 SO and SR, and much greater in these regions than in the middle and outer molecular layers of the DG ($P = 0.0001$ one-way ANOVA; $P \leq 0.001$ for dentate middle and outer molecular layers *vs.* CA1 SR in planned *post hoc* comparisons) (Fig. 5*C*).

We next used two-photon microscopy to determine whether the apparent homogeneity of CD73 immunolabelling seen in the dendritic layers of field CA1 in wide field microscopy extends down to the level at which individual spines and synapses are evident. This is not an unreasonable expectation given the evidence obtained from electron microscopy indicating that the enzyme is localized on glial membranes (Kreutzberg *et al.* 1978), which can be assumed to be distributed in a uniform manner throughout the neuropil. However, there remains the possibility that CD73 is not evenly distributed along membranes, a situation that could result in localized patches of labelling at the micron range.

Reconstruction of image z-stacks collected at 63× with a two-photon microscope demonstrated that immunoreactivity in SR was concentrated in large numbers of small (∼1 μm) clusters of variable size. The clusters were evenly distributed across the neuropil except for striations corresponding in orientation and size to pyramidal cell dendrites (Fig. 5*D*) and open areas occupied by cell bodies. There was no evidence for dense labelling inside structures with anatomical features of glial or neuronal cell bodies. In sum, the high-resolution immunostaining pattern suggests a broadly distributed enzyme that concentrates around structures with the size and frequency characteristics of dendritic spines.

Theta processing and adenosine modulation in the piriform cortex

We next investigated whether either of the two response profiles found in the hippocampus are representative of a typical pattern in the cortical forebrain. The piriform cortex innervates the LEC that, in turn, generates the LPP input to the DG (Wilson & Sullivan, 2011). It therefore represents a logical site for making comparisons with the hippocampus. Moreover, afferents to the superficial layer of the piriform cortex are laminated, with the LOT terminating in layer 1a and associational afferents restricted to layer 1b (Luskin & Price, 1983). The sharp boundary between the lamina, and between the molecular layer and cell body layer (layer 2), greatly simplifies the problem of selectively stimulating either afferent population.

As in previous studies using acute slices (Jung *et al.* 1990) and *in vivo* recordings (McNamara *et al.* 2004), LOT synapses in layer 1a generated a conventional PPF effect, whereas associational contacts in layer 1b did not (Fig. 6*A*). Input/output curves (stimulation intensity *vs.* initial slope of fEPSP) for LOT and associational inputs were not statistically different (Fig. 6*B*) and were similar to those collected for the LPP. Examination of individual traces (Fig. 6*B*, inset), however, indicated that the decay phase of the LOT progressively diverged from ASSN responses with an increasing stimulation intensity ($P = 0.003$, two-way repeated measures ANOVA, $F_{9117} = 2.962$) (Fig. 6*C*). The best interpretation of these results is that, because of greater proximity to layer 2 and 3 cell bodies, large associational responses have a greater probability of triggering action potentials than do responses of the same size in the more distal layer 1a.

By contrast to the similar I/O results, the innervation of layers 1a and 1b responded very differently to theta stimulation. A 20 s train applied to the LOT produced

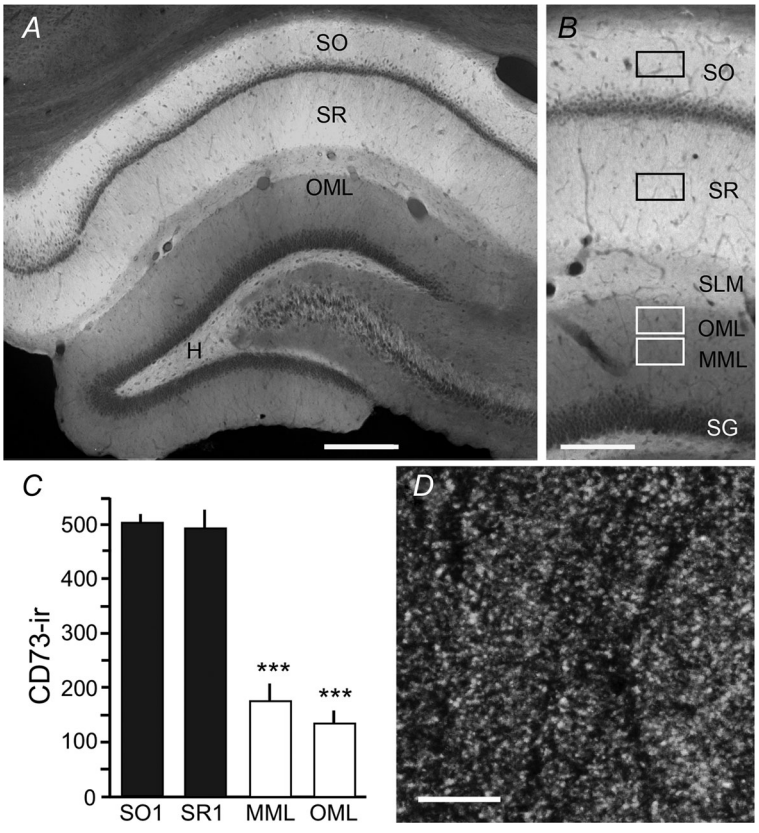

Figure 5. Distribution of CD73 immunoreactivity in the rostral hippocampus
A, montage, and higher magnification image (*B*), showing that CD73 immunoreactivity is particularly dense in field CA1 SO and SR, less so in CA1 stratum lacunosum moleculare (SLM) and the subgranular hilus (H), and very low in the dentate molecular layer (OLM, outer molecular layer; MML, middle molecular layer; SG, stratum granulosum). *C*, measures of immunofluorescence intensity show differences in relative levels of CD73 immunoreactivity (above corpus callosum values) in CA1 strata oriens (SO1) and radiatum (SR1) and the dentate MML and OML (sample field placement is indicated by boxes in *B*); laminar density measures were significantly different (***$P \leq 0.0001$, one-way ANOVA). *D*, two photon image shows that CD73 immunoreactivity is localized to puncta evenly distributed across the neuropil of CA1 SR. Image acquired in region noted with black square box in (*B*). Scale bar = 300 μm for (*A*), 170 μm for (*B*) and 5 μm for (*D*).

a time varying pattern comparable to that seen in the LPP: the second response was substantially increased above baseline, although subsequent pulses produced progressively less enhancement such that facilitation was absent by the seventh second of the train. Responses to associational stimulation were unique in that there was no initial facilitation but rather a steady decrease, resulting in responses that were substantially smaller than baseline; in essence, there was no frequency facilitation but only depression at the theta frequency (Fig. 6*D*).

In sum, two of the three variables discussed earlier (input/output curves, theta processing) served to establish similarities between LOT innervation of the piriform cortex and the LPP projection to the DG; the latter variable clearly distinguished the associational projections from other connections. The results obtained in the piriform cortex for the third factor (i.e. adenosine modulation) were striking. The calcium-binding protein calretinin is present at very high concentrations in the LOT projections (Jacobowitz & Winsky, 1991). We used this protein marker to delineate the LOT and the limits of its terminal field in the piriform cortex (Fig. 7*A*). The cell sparse outer margin of the tissue (Fig. 7*Ai*), corresponding to the LOT proper, was densely immunolabelled for calretinin, as was the subjacent 150 μm of layer 1a (Fig. 7*Aii*); the inner boundary of the latter field was quite sharp, in agreement with the known restriction of LOT synapses to piriform layer 1a. Immunostaining for CD73 (Fig. 7*Aiii*) aligned with the LOT terminal zone in layer 1a but was absent from layer 1b. These results indicate that an essential enzyme for extracellular production of adenosine is present at high levels in the lamina innervated by the LOT but largely absent from that targeted by the piriform associational system.

Infusion of almost threshold levels of the A1R antagonist DPCPX had markedly different effects on baseline responses in the two populations of piriform synapses: it elicited a pronounced increase in slope and amplitude of LOT fEPSPs in layer 1a (34.2 $\pm$ 3.7% at 30 min into drug treatment; $P = 0.02$, two-tailed paired t test against baseline) and had no evident effect on the associational innervation of layer 1b (Fig. 7*B*). The difference in the effect of the drug on the two pathways was highly significant ($P < 0.01$, two-tailed t test, last 5 min of ASSN *vs.* last 5 min of LOT). Thus, as in the hippocampus, fields with high concentrations of CD73 are associated with clear evidence for adenosine modulation in the piriform cortex.

Finally, we used the NTPDase inhibitor POM-1 (Wall *et al.* 2008; Wall & Dale, 2013) to test the prediction that inhibition of extracellular ATP metabolism produces an increase in the size of LOT responses. Infusion of the compound at 30 μM caused a modest but stable increase in LOT responses ($P < 0.012$, two-tailed t test, last 1 min of baseline *vs.* the fiftieth minute of POM-1 infusion). This effect occluded that of DPCPX (Fig. 7*C*). These results are consistent with the conclusion that, in the LOT terminal field, as in the hippocampus (Wall & Dale, 2013), activity-induced increases in extracellular adenosine derive from both metabolism of released ATP (blocked by POM-1) and direct adenosine release.

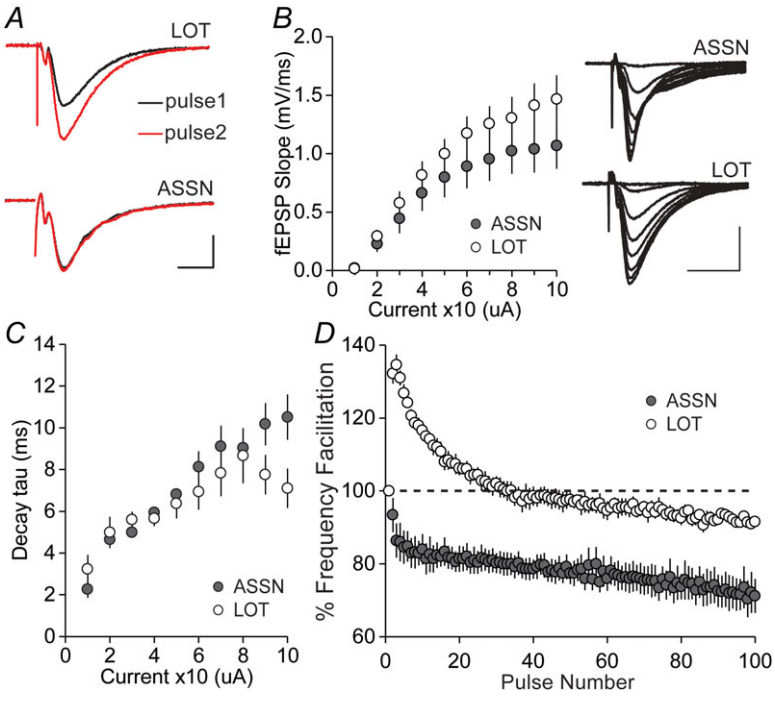

Figure 6. Characterization of baseline synaptic transmission in the LOT and ASSN projections within the piriform cortex
A, representative traces of paired-pulse (40 ms interval) responses. PPF is observed in LOT but not in ASSN projections. Scale bar = 1 mV/5 ms. *B*, input/output curves compare the initial slope of the fEPSP with the amount of current delivered to LOT and ASSN afferents. Inset: representative traces of input/output fEPSP recordings. Scale bar = 1 mV/10 ms. *C*, input/output curves for decay tau (ms) of the fEPSP to current delivered to LOT and ASSN afferents. *D*, LOT responses to a 20 s theta pulse train showed an immediate facilitation that steadily decayed toward baseline. ASSN responses did not show enhancement and became progressively smaller during the train.

Theta processing at the remaining links in the piriform-hippocampal network

The results described thus far differentiate two pathways in the hippocampus, with associated mechanisms, and include comparisons for key features with two populations of synapses in the piriform cortex. The results for these four connections provide a starting point for investigating whether differential signal transformations across network links result in a coherent output. Accordingly, we examined the frequency responses to a theta train in three additional connections from piriform cortex to CA1.

Layer II pyramidal neurons of the LEC receive the majority of their afferents from the posterior piriform cortex (Kerr *et al.* 2007), essentially an extension of the piriform associational system, and generate the LPP; thus, they constitute the third step in the piriform-hippocampal network. We developed a slice preparation for the region using sections through the temporal portion of the hippocampal complex and analysed fEPSPs with recording and stimulating electrodes placed in layer 1b, the terminal zone for piriform projections (Fig. 8*A*). Synaptic responses were relatively small, not unlike those recorded in the piriform associational system. Theta stimulation had only small effects on fEPSPs: there was a very weak initial facilitation followed by a decline during the 20 s train to values that were below baseline (Fig. 8*B*). This pattern resembled that for the piriform associational system, except for the first 2–3 s of the train.

The dense associational connections within field CA3 constitute a stage in the network, as well as providing collaterals that constitute the final link to field CA1. We tested theta processing using stimulation and recording electrodes placed in the proximal SR, the termination zone for the apical branch of the CA3 associational system (Fig. 8*C*). Responses to the first 3 s of the theta train

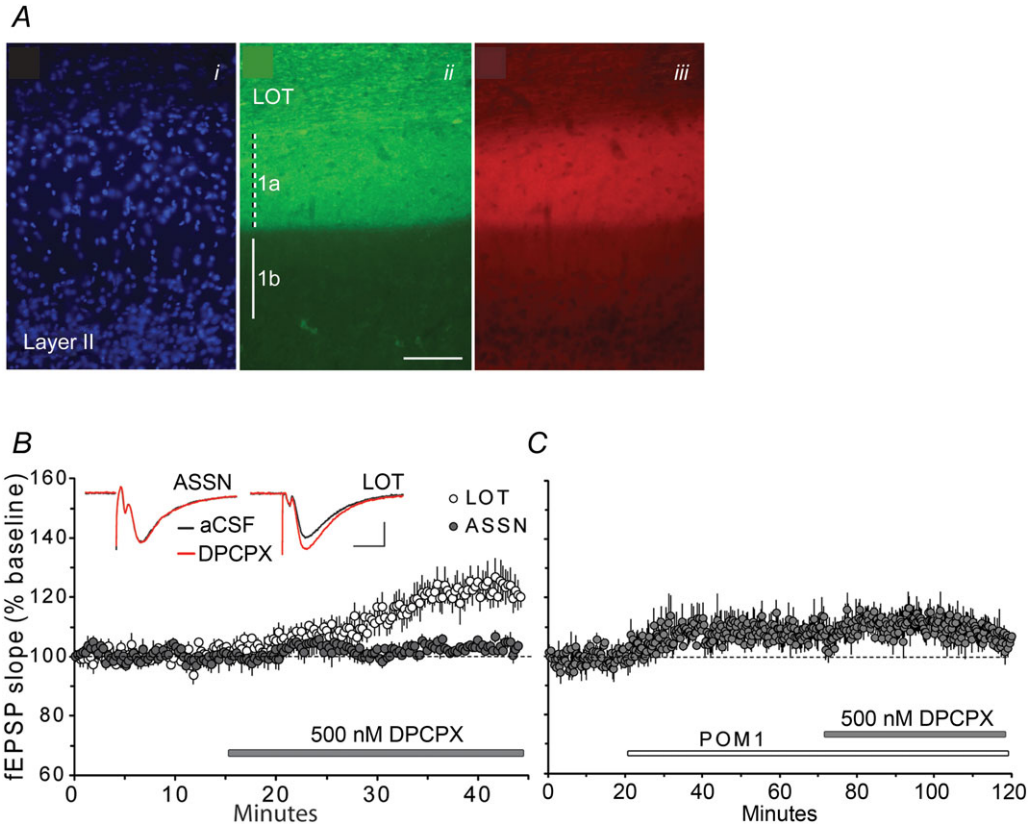

Figure 7. CD73 distribution and adenosine modulation in the piriform cortex
A, sections through the piriform cortex were processed for immunofluorescence localization of CD73 and calretinin, a calcium-binding protein concentrated within olfactory bulb afferents of the piriform cortex. Images of the same piriform cortex field show 4′,6-diamidino-2-phenylindole-labelled cell nuclei (*i*), calretinin immunoreactivity (*ii*) and CD73 immunoreactivity (*iii*). Calretinin immunoreactivity was dense within the LOT and its terminal field in layer 1a but absent from layer 1b (*ii*). Similarly, CD73 immunoreactivity is present at high concentrations in layer 1a but absent from layer 1b (*iii*). Scale bar = 100 μm. *B*, infusions of the A1R antagonist DPCPX (grey bar) caused a significant enhancement in baseline synaptic transmission in LOT ($n = 4$) but not in ASSN projections ($n = 4$). Inset: representative traces of fEPSPs collected during baseline (aCSF) and 30 min after start of DPCPX infusion. Scale bar = 0.5 mV/5 ms. *C*, NTPDase inhibitor, POM-1, increases synaptic transmission in LOT and largely occludes the effect of DPCPX ($n = 4$).

produced a frequency facilitation pattern very similar to that found in CA1 (an increase in fEPSPs followed by a decline), although the prominent secondary facilitation in the latter field was absent in CA3 (Fig. 8*D*).

The mossy fibres from the granule cells to the field CA3 pyramidal neurons are a salient link in the cortico-hippocampal network. Frequency facilitation has been investigated in detail in previous extracellular and intracellular recording studies and found to be markedly greater than at other sites in the hippocampus (Regehr *et al.* 1994; Geiger & Jonas, 2000; Feng *et al.* 2003; Nicoll & Schmitz, 2005). We collected the results for theta by stimulating the projections at a site immediately beneath the granule cells, well outside the CA3-associational projections (Fig. 8*E*). In accordance with previous studies of mossy fibres, we found that infusion of DCG-IV (1 μM), a group II mGluR agonist, caused a robust depression of fEPSPs to <70% of baseline amplitude (Kamiya *et al.* 1996). Frequency facilitation was as expected from prior work (Regehr *et al.* 1994; Geiger & Jonas, 2000) but, in the present study, it was shown to follow a negatively accelerating trajectory; the first 3 s produced rapid facilitation to 250 ± 26% and then responses steadily facilitated to 315 ± 34% at the end of 20 s (Fig. 8*F*).

Discussion

The present study has identified three aspects of synaptic function (i.e. signal processing, plasticity, and purinergic modulation) that differentiate sequential stages across a cortico-hippocampal network and probably result in specific roles for these relays in information processing and storage. The DG emerged as a relatively passive structure, at least relative to CA1. fEPSP facilitation occurred during the early phase of a theta train but then steadily decayed as stimulation continued. Adenosine modulation of the

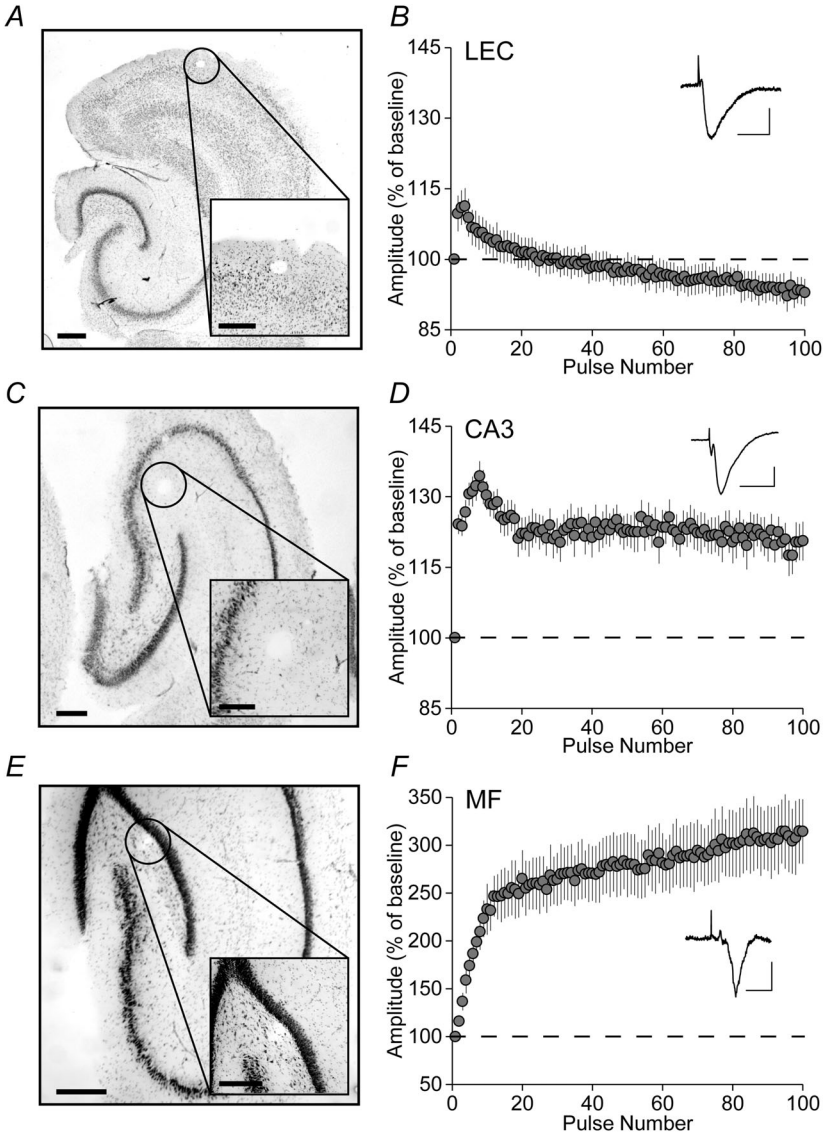

Figure 8. Theta trains produce different facilitation patterns in LEC, CA3 and mossy fibres (MF)
A, Nissl (cresyl violet) stain of hippocampus with attached entorhinal cortex showing the location of a stimulating electrode in layer 1b of the LEC. Scale bar = 0.65 mm. Inset: magnified image of electrode placement. Scale bar = 0.30 mm. *B*, 20 s of theta pulse stimulation results in weak facilitation of fEPSP amplitude, which slowly decays to slightly below baseline (n = 6). Inset: representative fEPSP trace during baseline stimulation. Scale bar = 0.25 mV/10 ms. *C*, Nissl stain showing stimulating electrode placement in area CA3b SR. Scale bar = 0.36 mm. Inset: magnified image of electrode placement. Scale bar = 0.2 mm. *D*, 20 s of theta pulse stimulation of the CA3 associational system results in an initial facilitation phase similar to that in field CA1 but lacking the biphasic pattern found in that region (n = 12). Inset: representative fEPSP trace during baseline stimulation. Scale bar = 0.5 mV/10 ms. *E*, Nissl stain showing stimulating electrode placement adjacent to the DG granule cell layer in the hilus. Scale bar = 0.37 mm. Inset: magnified image of electrode placement. Scale bar = 0.33 mm. *F*, 20 s of theta pulse stimulation of the mossy fibres results in rapid facilitation to 250 ± 26% of baseline amplitude after 3 s and then a slower but still increasing facilitation until the end of the train (n = 5). Inset: representative fEPSP trace during baseline stimulation. Scale bar = 0.25 mV/5 ms.

responses was weak and LTP induction required HFS of large numbers of axons. The S-C projections behaved in a much more dynamic manner. Theta trains generated two phases of facilitation, the second of which persisted across 20 s of stimulation. Adenosine modulation in CA1 was apparent and robust LTP required minimal, naturalistic patterns of stimulation, which are features that were lacking in the LPP.

Factors probably involved in each of the region-specific effects were identified. The S-C projections possessed secondary transmitter mobilization capacities, not found in the LPP, which account for differences in frequency facilitation and had much steeper I/O curves than the LPP-DG connection, a distinction logically related to the number of activated afferents needed to engage NMDA receptor-dependent LTP. In accordance with this argument, voltage clamping eliminated the LTP threshold differences between the DG and CA1. The dissimilar I/O curves are not unexpected given that the entorhinal-DG projections are divergent (Haberly, 2001; Wilson & Sullivan, 2011), whereas the S-C system is not (Ishizuka *et al.* 1990). Finally, the presence (CA1) *vs.* the absence (DG) of adenosine modulation of theta train responses corresponded to regional differences in levels of the CD73 that converts released ATP into the purine (Cunha, 2001; Lovatt *et al.* 2012). It should be noted that the 5 Hz trains were delivered against a 3 pulses min^{-1} level of background stimulation. An intriguing issue for future research will be to determine whether constantly changing patterns of afferent activity, as occur during behaviour, modify the facilitation produced by seconds long periods of theta activity.

The marked disparity in adenosine involvement also differentiated facets of LTP in the two nodes of the intrahippocampal circuit. It is well established that theta stimulation erases recently induced LTP in field CA1 (Staubli & Lynch, 1990) and that this effect is mediated by endogenous adenosine acting through A1Rs (Larson *et al.* 1993; Abraham & Huggett, 1997; Huang *et al.* 1999). As described in the present study, the LTP reversal effect is not present in the CD73-poor DG. Clearly, the DG has the receptor mechanisms necessary for reversal because infusions of the adenosine analogue 2-CAD, applied shortly after induction, eliminated LTP in the LPP. Thus, it appears that theta trains fail to increase extracellular adenosine in the DG to levels needed to erase potentiation. The presence or absence of physiologically plausible means for modifying newly formed LTP could relate to the above observations concerning differences in LTP thresholds. A system capable of forming associations with minimal training (CA1) is prone to errors (encoding irrelevant information) and so requires a *post hoc* correction mechanism, whereas an area (DG) that requires multiple trials will exclude elements that are not reliable constituents of the environment.

Having identified clear differences in signal processing and plasticity at sites within hippocampus, we next investigated whether either of these response profiles predominates in the piriform cortex, an associational type cortex that is a primary source of entorhinal cortex afferents. Within-theta facilitation of the LOT more closely

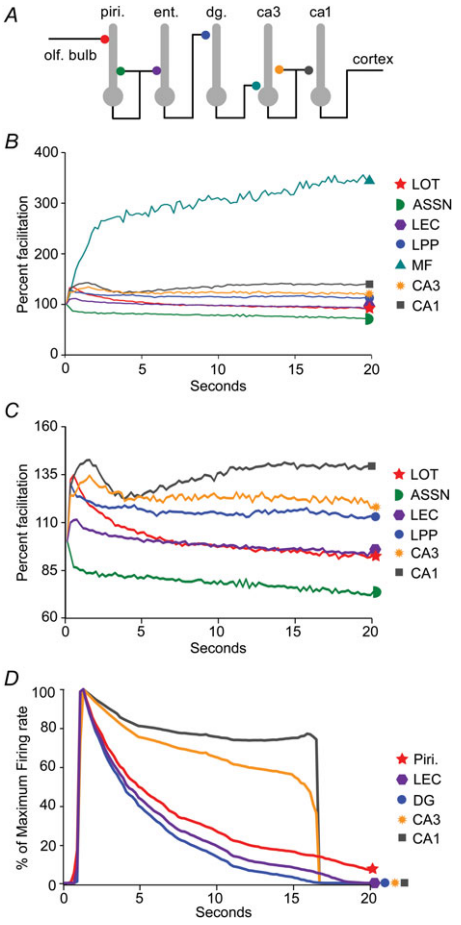

Figure 9. A model of the seven-stage network with local response facilitation characteristics
A, schematic of the network extending from the LOT through the output from hippocampal field CA1. *B*, summary of response facilitation during a 20 s long period of theta pulse stimulation for the seven network stages described in (*A*). As expected, theta responses facilitated to a much greater degree in the mossy fibres (MF) than in the other pathways. *C*, as in (*B*) but with the mossy fibre curve removed. Over time, changes in fEPSPs differed across the network nodes. The piriform associational projections (piri.) exhibited an unusual depression effect, whereas their extension into the LEC changed only slightly after a brief, weak facilitation. The other four synaptic populations facilitated to approximately the same degree at the beginning of theta but then followed different temporal patterns for the remainder of the train. *D*, neuronal activity in five network nodes as generated by the simulation described in the main text. Firing in a given stage is normalized to the peak rate for that stage. Activity in first three links declined rapidly after a brief facilitation, with the severity of the change increasing from the piriform cortex to DG. The output of the system (CA1) was unexpectedly stable for 17 s of the theta train and then abruptly fell to zero.

resembled the LPP than CA1, whereas the associational system exhibited progressive depression. I/O curves for the two piriform projections were comparable to that for the DG, an observation in accordance with the conclusion that relatively flat curves are typical of divergent projections. The olfactory bulb mitral cells are far less numerous than their target piriform neurons, and associational fibres from a given site travel throughout the entire olfactory cortex (Haberly, 2001; Wilson & Sullivan, 2011); basically, both projections are highly divergent and, in this respect, similar to the perforant path. Previous studies have shown that the threshold for LTP was higher for the divergent projections in the piriform cortex (Jung *et al.* 1990) than for the non-divergent S-C system.

The association of high concentrations of CD73 with adenosine modulation found in the hippocampus was confirmed for the superficial piriform cortex, being evident for the LOT but not the associational projections. The functional significance of radically different levels of adenosine modulation within adjacent lamina in the same dendritic field is an intriguing issue. The LOT carries primary sensory information and adenosine-mediated suppression of transmission during many seconds of sampling could produce a type of habituation, an effect that would encourage cue switching. The unusual frequency depression effect in the associational system would then be expected to accentuate the loss ('habituation') of piriform output after initial sampling.

The piriform data extend the analysis of local processing to four components of one of the better defined, in anatomical terms, multistage networks found in the mammalian forebrain (Fig. 9*A*). Questions then arise about the magnitude of differences in signal processing across the entire seven link system and the type of output that emerges from the various signal transformations performed by its serial components. Accordingly, we tested for response facilitation to theta stimulation in the piriform projections to the LEC, the mossy fibre connection between the granule cells and field CA3, and the intra-CA3 associational system. These additional data (Fig. 9*B* and *C*) provided the material needed to construct a model for investigating what the output of a long cortical network with highly differentiated serial steps might look like.

We constructed a simulation using the data from Fig. 9*B* and *C*; synaptic weights were constant across nodes, except for the mossy fibres (3×) and, in line with anatomical and I/O results, connectivity was higher for the pyramidal cell fields than elsewhere. The realism of modelling exercises is limited by the small number of neurons that can be simulated; moreover, the very complex system tends to be unstable. This problem was resolved using minor adjustments to the size, duration and connectivity of inhibitory connections in the CA3 region. With these limitations in mind, the model does accurately incorporate, at single synapses, the diverse response facilitation curves shown in Fig. 9*B* and *C*.

For comparison purposes, over time, firing for each node during a 20 s theta input was normalized to the peak firing for that node. Firing increased rapidly during the first 0.5 s of input and then declined; the latter effect differed markedly between network stages (Fig. 9*D*). The piriform-lateral entorhinal segments decreased to ∼50% of peak values within the first 5 s of theta. Activity in the DG underwent an even greater drop. These changes reflect (i) relatively weak or even negative response facilitation at individual contacts and (ii) the divergent, sparse (relative to CA3) nature of the piriform associational system. Unexpectedly, given the marked regional differences in response facilitation, CA1 output was maintained at a high level for most of the train. The pronounced mossy fibre facilitation at theta frequency (Fig. 9*B*), coupled with the relatively dense connectivity of the recurrent CA3 associational projections, was largely responsible for supporting activity in the face of rapidly decreasing granule cell firing. Earlier work with diverse models suggested that CA3 is capable of autonomous activity for several seconds (Tateno *et al.* 1998; Renno-Costa *et al.* 2014). Output collapsed at ∼17 s because input from earlier stages had reached very low values.

In sum, the different signal transformations occurring across network stages, when combined with local anatomical features, result in a three temporal phases of operation: (i) high output from all components for ∼1 s; (ii) a period from ∼3 s to 15 s during which the output of CA3 and CA1 is markedly greater than that from the upstream components (piriform-entorhinal); and (iii) a sudden, non-linear decay in the former.

The piriform cortex, although treated thus far in terms of relays, sends major projections to the amygdala, frontal cortex, striatum and other telencephalic regions. We propose that the shift from front-end (LOT though DG) to back-end processing during extended theta activity provides the network with the flexibility needed to deal with different types of problems. For example, the system is required to discriminate between multiple, now present cues, at the same time as being able to track particular stimuli (odours) to sources. The first activity involves short, repetitive sampling episodes allowing for brief periods during which LOT and DG facilitation are maximal. The latter requires movement through extended space and maintenance of representations for the many seconds needed to follow a signal that will vary in intensity under real world conditions.

The three variables that describe regional differentiation influence local plasticity as well as theta throughput. It is therefore possible that the properties of LTP, including reversal, differ markedly between network links in the manner found for response facilitation. Comparisons between the DG and CA1 described in the present study

encourage this possibility. The existence of widespread differences in plasticity would be relevant to the hypothesis that variations between nodes are a prerequisite for a multipurpose network. For example, encoding of cues in the piriform-entorhinal components might be best accomplished using sampling strategies other than those appropriate for CA3-CA1. The modelling work already suggests something of this sort. The rapid decay of response facilitation in the early nodes indicates that multiple, short sampling periods and repeated LTP episodes represent effective means for encoding. Conversely, maintenance of high levels of facilitation in the pyramidal cell fields, as found in the model, would create a ready state for synaptic modifications that persist throughout a long search. This could be essential for associating an odour representation with visual cues (an object or location) that arrive, via the medial perforant path, after an unpredictable interval.

In summary, this first multivariate analysis indicates that the multiple stages of a cortico-hippocampal network, although serving as relays from the periphery to the cortex, have markedly different properties. In the present case, it is argued that these differences allow the network to perform different types of operations: learning and discrimination of cues *vs.* tracking and multimodal association.

References

Abraham WC & Huggett A (1997). Induction and reversal of long-term potentiation by repeated high-frequency stimulation in rat hippocampal slices. *Hippocampus* **7**, 137–145.

Abraham WC, Mason-Parker SE & Logan B (1996). Low-frequency stimulation does not readily cause long-term depression or depotentiation in the dentate gyrus of awake rats. *Brain Res* **722**, 217–221.

Arai A, Kessler M & Lynch G (1990). The effects of adenosine on the development of long-term potentiation. *Neurosci Lett* **119**, 41–44.

Arima-Yoshida F, Watabe AM & Manabe T (2011). The mechanisms of the strong inhibitory modulation of long-term potentiation in the rat dentate gyrus. *Eur J Neurosci* **33**, 1637–1646.

Barrionuevo G, Schottler F & Lynch G (1980). The effects of repetitive low-frequency stimulation on control and potentiated synaptic responses in the hippocampus. *Life Sci* **27**, 2385–2391.

Boss BD, Peterson GM & Cowan WM (1985). On the number of neurons in the dentate gyrus of the rat. *Brain Res* **338**, 144–150.

Bramham CR, Milgram NW & Srebro B (1991). Delta opioid receptor activation is required to induce LTP of synaptic transmission in the lateral perforant path in vivo. *Brain Res* **567**, 42–50.

Bramham CR & Sarvey JM (1996). Endogenous activation of mu and delta-1 opioid receptors is required for long-term potentiation induction in the lateral perforant path: dependence on GABAergic inhibition. *J Neurosci* **16**, 8123–8131.

Breindl A, Derrick BE, Rodriguez SB & Martinez JL (1994). Opioid receptor-dependent long-term potentiation at the lateral perforant path-CA3 synapse in rat hippocampus. *Brain Res Bull* **33**, 17–24.

Christie BR & Abraham WC (1994). Differential regulation of paired-pulse plasticity following LTP in the dentate gyrus. *Neuroreport* **5**, 385–388.

Colgin LL (2013). Mechanisms and functions of theta rhythms. *Annu Rev Neurosci* **36**, 295–312.

Colgin LL, Jia YS, Sabatier JM & Lynch G (2005). Blockade of NMDA receptors enhances spontaneous sharp waves in rat hippocarnpal slices. *Neurosci Lett* **385**, 46–51.

Colgin LL, Kramar EA, Gall CM & Lynch G (2003). Septal modulation of excitatory transmission in hippocampus. *J Neurophysiol* **90**, 2358–2366.

Colino A & Malenka RC (1993). Mechanisms underlying induction of long-term potentiation in rat medial and lateral perforant paths in vitro. *J Neurophysiol* **69**, 1150–1159.

Cunha RA (2001). Regulation of the ecto-nucleotidase pathway in rat hippocampal nerve terminals. *Neurochem Res* **26**, 979–991.

Debanne D, Guerineau NC, Gahwiler BH & Thompson SM (1996). Paired-pulse facilitation and depression at unitary synapses in rat hippocampus: quantal fluctuation affects subsequent release. *J Physiol London* **491**, 163–176.

Demendonca A & Ribeiro JA (1990). 2-Chloroadenosine decreases long-term potentiation in the hippocampal CA1 area of the rat. *Neurosci Lett* **118**, 107–111.

Dolphin AC (1983). The adenosine agonist 2-chloroadenosine inhibits the induction of long-term potentiation of the perforant path. *Neurosci Lett* **39**, 83–89.

Dudek SM & Bear MF (1992). Homosynaptic long-term depression in area CA1 of hippocampus and effects of N-methyl-D-aspartate receptor blockade. *Proc Natl Acad Sci USA* **89**, 4363–4367.

Dunwiddie T & Lynch G (1978). Long-term potentiation and depression of synaptic responses in rat hippocampus – localization and frequency dependency. *J Physiol London* **276**, 353–367.

Dunwiddie TV & Haas HL (1985). Adenosine increases synaptic facilitation in the in vitro rat hippocampus – evidence for a presynaptic site of action. *J Physiol London* **369**, 365–377.

Feng L, Molnar P & Nadler JV (2003). Short-term frequency-dependent plasticity at recurrent mossy fiber synapses of the epileptic brain. *J Neurosci* **23**, 5381–5390.

Geiger JRP & Jonas P (2000). Dynamic control of presynaptic Ca^{2+} inflow by fast-inactivating K^{+} channels in hippocampal mossy fiber boutons. *Neuron* **28**, 927–939.

Gocel J & Larson J (2013). Evidence for loss of synaptic AMPA receptors in anterior piriform cortex of aged mice. *Front Aging Neurosci* **5**, 39.

Haberly LB (2001). Parallel-distributed processing in olfactory cortex: new insights from morphological and physiological analysis of neuronal circuitry. *Chem Senses* **26**, 551–576.

Han ZS, Buhl EH, Lorinczi Z & Somogyi P (1993). A high-degree of spatial selectivity in the axonal and dendritic domains of physiologically identified local-circuit neurons in the dentate gyrus of the rat hippocampus. *Eur J Neurosci* **5**, 395–410.

Henze DA, Urban NN & Barrioneuvo G (2000). The multifarious hippocampal mossy fiber pathway: a review. *Neuroscience* **98**, 407–427.

Huang CC, Liang YC & Hsu KS (1999). A role for extracellular adenosine in time-dependent reversal of long-term potentiation by low-frequency stimulation at hippocampal CA1 synapses. *J Neurosci* **19**, 9728–9738.

Hunsaker MR & Kesner RP (2013). The operation of pattern separation and pattern completion processes associated with different attributes or domains of memory. *Neurosci Biobehav R* **37**, 36–58.

Ishizuka N, Weber J & Amaral DG (1990). Organization of intrahippocampal projections originating from CA3 pyramidal cells in the rat. *J Comp Neurol* **295**, 580–623.

Jacobowitz DM & Winsky L (1991). Immunocytochemical localization of calretinin in the forebrain of the rat. *J Comp Neurol* **304**, 198–218.

Jain S, Yoon SY, Zhu L, Brodbeck J, Dai J, Walker D & Huang YD (2012). Arf4 determines dentate gyrus-mediated pattern separation by regulating dendritic spine development. *PLoS One* **7**, e46340.

Jung MW, Larson J & Lynch G (1990). Long-term potentiation of monosynaptic EPSPs in rat piriform cortex in vitro. *Synapse* **6**, 279–283.

Kamiya H, Shinozaki H & Yamamoto C (1996). Activation of metabotropic glutamate receptor type 2/3 suppresses transmission at rat hippocampal mossy fibre synapses. *Journal Physiol* **493**, 447–455.

Kerr KM, Agster KL, Furtak SC & Burwell RD (2007). Functional neuroanatomy of the parahippocampal region: the lateral and medial entorhinal areas. *Hippocampus* **17**, 697–708.

Kesner RP, Lee I & Gilbert P (2004). A behavioral assessment of hippocampal function based on a subregional analysis. *Rev Neuroscience* **15**, 333–351.

Kramar EA, Babayan AH, Gavin CF, Cox CD, Jafari M, Gall CM, Rumbaugh G & Lynch G (2012). Synaptic evidence for the efficacy of spaced learning. *Proc Natl Acad Sci USA* **109**, 5121–5126.

Kramar EA, Bernard JA, Gall CM & Lynch G (2002). Alpha3 integrin receptors contribute to the consolidation of long-term potentiation. *Neuroscience* **110**, 29–39.

Kramar EA & Lynch G (2003). Developmental and regional differences in the consolidation of long-term potentiation. *Neuroscience* **118**, 387–398.

Kreutzberg GW, Barron KD & Schubert P (1978). Cytochemical-localization of 5'-nucleotidase in glial plasma-membranes. *Brain Res* **158**, 247–257.

Larson J, Wong D & Lynch G (1986). Patterned Stimulation at the theta-frequency is optimal for the induction of hippocampal long-term potentiation. *Brain Res* **368**, 347–350.

Larson J, Xiao P & Lynch G (1993). Reversal of LTP by theta frequency stimulation. *Brain Res* **600**, 97–102.

Lee KS, Schubert P, Reddington M & Kreutzberg GW (1986). The distribution of adenosine A1 receptors and 5'-nucleotidase in the hippocampal formation of several mammalian species. *J Comp Neurol* **246**, 427–434.

Leutgeb JK, Leutgeb S, Moser MB & Moser EI (2007). Pattern separation in the dentate gyrus and CA3 of the hippocampus. *Science* **315**, 961–966.

Leutgeb S & Leutgeb JK (2007). Pattern separation, pattern completion, and new neuronal codes within a continuous CA3 map. *Learn Memory* **14**, 745–757.

Lovatt D, Xu QW, Liu W, Takano T, Smith NA, Schnermann J, Tieu K & Nedergaard M (2012). Neuronal adenosine release, and not astrocytic ATP release, mediates feedback inhibition of excitatory activity. *Proc Natl Acad Sci USA* **109**, 6265–6270.

Luskin MB & Price JL (1983). The topographic organization of associational fibers of the olfactory system in the rat, including centrifugal fibers to the olfactory-bulb. *J Comp Neurol* **216**, 264–291.

Macek TA, Winder DG, Gereau RW, Ladd CO & Conn PJ (1996). Differential involvement of group II and group III mGluRs as autoreceptors at lateral and medial perforant path synapses. *J Neurophysiol* **76**, 3798–3806.

Manabe T, Wyllie DJA, Perkel DJ & Nicoll RA (1993). Modulation of synaptic transmission and long-term potentiation – effects on paired-pulse facilitation and EPSC variance in the CA1 Region of the hippocampus. *J Neurophysiol* **70**, 1451–1459.

Martin SJ (1998). Time-dependent reversal of dentate LTP by 5 Hz stimulation. *Neuroreport* **9**, 3775–3781.

McNamara AM, Cleland TA & Linster C (2004). Characterization of the synaptic properties of olfactory bulb projections. *Chem Senses* **29**, 225–233.

Megias M, Emri Z, Freund TF & Gulyas AI (2001). Total number and distribution of inhibitory and excitatory synapses on hippocampal CA1 pyramidal cells. *Neuroscience* **102**, 527–540.

Min MY, Asztely F, Kokaia M & Kullmann DM (1998). Long-term potentiation and dual-component quantal signaling in the dentate gyrus. *Proc Natl Acad Sci USA* **95**, 4702–4707.

Molter C, O'Neill J, Yamaguchi Y, Hirase H & Leinekugel X (2012). Rhythmic modulation of theta oscillations supports encoding of spatial and behavioral information in the rat hippocampus. *Neuron* **75**, 889–903.

Newman EL & Hasselmo ME (2014). CA3 sees the big picture while dentate gyrus splits hairs. *Neuron* **81**, 226–228.

Nicoll RA & Schmitz D (2005). Synaptic plasticity at hippocampal mossy fibre synapses. *Nat Rev Neurosci* **6**, 863–876.

Niewoehner B, Single FN, Hvalby O, Jensen V, Borgloh SMZA, Seeburg PH, Rawlins JNP, Sprengel R & Bannerman DM (2007). Impaired spatial working memory but spared spatial reference memory following functional loss of NMDA receptors in the dentate gyrus. *Eur J Neurosci* **25**, 837–846.

Paxinos G & Watson C (1986). *Rat Brain.* In: *Stereotaxic Coordinates.* Academic Press Inc., San Diego, CA.

Preibisch S, Saalfeld S & Tomancak P (2009). Globally optimal stitching of tiled 3D microscopic image acquisitions. *Bioinformatics* **25**, 1463–1465.
Qin W & Yu CS (2013). Neural pathways conveying no visual information to the visual cortex. *Neural Plast* **1**, 14.
Regehr WG, Delaney KR & Tank DW (1994). The role of presynaptic calcium in short-term enhancement at the hippocampal messy fiber synapse. *J Neurosci* **14**, 523–537.
Renno-Costa C, Lisman JE & Verschure PF (2014). A signature of attractor dynamics in the CA3 region of the hippocampus. *PLoS Comput Biol* **10**, e1003641.
Rex CS, Chen LY, Sharma A, Liu JH, Babayan AH, Gall CM & Lynch G (2009). Different Rho GTPase-dependent signaling pathways initiate sequential steps in the consolidation of long-term potentiation. *J Cell Biol* **186**, 85–97.
Rex CS, Kramar EA, Colgin LL, Lin B, Gall CM & Lynch G (2005). Long-term potentiation is impaired in middle-aged rats: regional specificity and reversal by adenosine receptor antagonists. *J Neurosci* **25**, 5956–5966.
Rolls ET (2013). The mechanisms for pattern completion and pattern separation in the hippocampus. *Front Syst Neurosci* **7**, 74.
Schneider CA, Rasband WS & Eliceiri KW (2012). NIH Image to ImageJ: 25 years of image analysis. *Nat Methods* **9**, 671–675.
Schoen SW & Kreutzberg GW (1994). Synaptic 5'-nucleotidase activity reflects lesion-induced sprouting within the adult rat dentate gyrus. *Exp Neurol* **127**, 106–118.
Staubli U, Larson J & Lynch G (1990). Mossy fiber potentiation and long-term potentiation involve different expression mechanisms. *Synapse* **5**, 333–335.
Staubli U & Lynch G (1990). Stable depression of potentiated synaptic responses in the hippocampus with 1–5 Hz stimulation. *Brain Res* **513**, 113–118.
Stimberg M, Goodman DF, Benichoux V & Brette R. (2014). Equation-oriented specification of neural models for simulations. *Front Neuroinform* **8**, 6.
Suzuki E & Okada T (2007). Regional differences in GABAergic modulation for TEA-induced synaptic plasticity in rat hippocampal CA1, CA3 and dentate gyrus. *Neurosci Res* **59**, 183–190.
Tateno K, Hayashi H & Ishizuka S (1998). Complexity of spatiotemporal activity of a neural network model which depends on the degree of synchronization. *Neural Networks* **11**, 985–1003.
Wall MJ & Dale N (2013). Neuronal transporter and astrocytic ATP exocytosis underlie activity-dependent adenosine release in the hippocampus. *J Physiol London* **591**, 3853–3871.
Wall MJ, Wigmore G, Lopatar J, Frenguelli BG & Dale N (2008). The novel NTPDase inhibitor sodium polyoxotungstate (POM-1) inhibits ATP breakdown but also blocks central synaptic transmission, an action independent of NTPDase inhibition. *Neuropharmacology* **55**, 1251–1258.
Weisskopf MG, Castillo PE, Zalutsky RA & Nicoll RA (1994). Mediation of hippocampal mossy fiber long-term potentiation by cyclic-AMP. *Science* **265**, 1878–1882.
Wilson DA & Sullivan RM (2011). Cortical Processing of Odor Objects. *Neuron* **72**, 506–519.
Wu LG & Saggau P (1994). Adenosine inhibits evoked synaptic transmission primarily by reducing presynaptic calcium influx in area CA1 of hippocampus. *Neuron* **12**, 1139–1148.
Zhang Y, Liu J, Luan G & Wang X (2015). Inhibition of the small GTPase Cdc42 in regulation of epileptic-seizure in rats. *Neuroscience* **289**, 381–391.

Additional information

Competing interests

The authors declare that they have no competing interests.

Author contributions

All experiments were performed at the University of California, Irvine. BHT, EAK, CDC, CMG and GL designed the study. BHT, EAK, CDC, YJ and WW performed the experiments and analysed the data. BHT, EAK, CDC, CMG and GL wrote the manuscript. All authors have read, commented on and approved the final version submitted for publication.

Funding

The research was supported in part by NSF grant #1146708 and ONR MURI grant N00014-10-1-0072 to GL and NIH grant NS45260 to CG and GL. CDC was supported by NSF predoctoral fellowship DGE0808392.

Acknowledgements

We thank Dr Julie C. Lauterborn and Bowen Hou for assistance in the analysis of CD73 immunolabelling.